JOURNAL OF GEOPHYSICAL RESEARCH, VOL. 106, NO. A12, PAGES 29,467–29,477, DECEMBER 1, 2001

# Excitation of low-frequency fluctuations at the magnetopause by intermittent broadband magnetosheath waves

J. De Keyser and V. Čadež

Belgian Institute for Space Aeronomy, Brussels, Belgium

**Abstract.** We study the excitation of magnetic field fluctuations at the magnetopause by incident low-frequency waves (frequencies below the ion gyrofrequency) that are highly intermittent and that have a broad frequency spectrum, like those observed in the magnetosheath. We present simulations of the transient response of the subsolar magnetopause to such magnetosheath waves in the context of linear resistive magnetohydrodynamics (MHD) in low-beta plasmas. The incident waves excite local Alfvén waves in resonant sheets within the magnetopause transition region wherever the condition for resonant MHD wave mode conversion is satisfied. Resonant sheet locations depend on the dominant frequencies in the incident wave spectrum. Because of the intermittency of the incident waves, the resonant sheets are rarely driven to saturation. The number of resonances, their position, their thickness, and the resonant wave amplitude all vary with time in response to the temporal changes in the incident wave spectra. The net result is that the low-frequency fluctuation level at the magnetopause is enhanced throughout the transition region rather than in a single or in a few resonant sheets, while the resonant amplitudes never reach excessively high values. This also implies that a fraction of the incident wave energy is resonantly absorbed throughout the magnetopause layer, instead of the very local absorption associated with an incident monochromatic wave. Resonances never develop into very narrow length scale structures, so that the MHD approach remains justified.

## 1. Introduction

Low-frequency plasma waves are present in many different space environments. In the present paper, we focus on waves with frequencies in the 0.01–1 Hz range (below the ion gyrofrequency) in the subsolar magnetosheath and magnetopause. Already in the early days of satellite exploration the Earth's magnetosheath was found to be filled with such low-frequency waves, while the magnetosphere is largely free of them [*Cahill and Amazeen*, 1963; *Ness et al.*, 1964; *Holzer et al.*, 1966; *Ness et al.*, 1966]. Later measurements confirmed this picture [*Engebretson et al.*, 1991] and demonstrated that the fluctuation level actually peaks in the magnetopause layer itself [*Perraut et al.*, 1979; *Rezeau et al.*, 1989; *Song et al.*, 1993]. Magnetosheath waves have a broad frequency content and they are very intermittent [*Anderson et al.*, 1982]. Magnetosheath wave observations have mostly been interpreted in the context of magnetohydrodynamics (MHD) [*Song et al.*, 1994]. Magnetosheath fluctuations have been reported to be often compressional, while fluctuations at the magnetopause appear to be Alfvénic [*Rezeau et al.*, 1989, 1993]. A review of low-frequency magnetosheath waves below, at, and slightly above the ion gyrofrequency is given by *Schwarz et al.* [1996]. Waves with frequencies above the ion gyrofrequency can only be understood by taking kinetic effects into account. Observations show that such non-MHD waves are often present [*Lacombe et al.*, 1995; *Anderson and Fuselier*, 1993].

Early studies of transmission and reflection of MHD waves at the magnetopause have shown that a large fraction of the incident waves is reflected, thus explaining the low fluctuation level in the magnetosphere [*McKenzie*, 1970; *Verzariu*, 1973]. Much work has focused on ultralow-frequency waves that might be responsible for magnetic pulsations [*Southwood*, 1974; *Engebretson et al.*, 1991]. Recently, attempts were made to explain the fluctuation level enhancement at the magnetopause. *Belmont et al.* [1995] proposed the following scenario: Waves present in the solar wind and amplified at the bow shock, or waves generated in the foreshock, can propagate downstream and reach the magnetopause, where they can be resonantly amplified because of wave mode conversion. Belmont et al. illustrated this scenario by discussing the propagation of a monochromatic incident wave in a low-beta plasma in the linear MHD approximation and found that depending on the incidence angle, the magnetosheath wave may either be partially transmitted and reflected, or partially absorbed and reflected. Absorption takes place in a narrow sheet where the incident wave resonantly excites an Alfvén wave; the magnetic field fluctuation amplitude in this sheet diverges for vanishing magnetic diffusion. *De Keyser et al.* [1999] demonstrated



Paper number 2001JA900078.
0148-0227/01/2001JA900078$09.00

how both Alfvén and slow waves can be resonantly excited when thermal pressure is not negligible, and how transmission and absorption can occur simultaneously.

There are basically two ways to tackle the wave propagation problem for general time-dependent incident waves in resistive MHD. A first technique relies on the Fourier transform to solve the problem in the frequency domain. Superposition of monochromatic wave results for a discrete number of frequencies that sample the spectrum of the driver then gives the desired result. The number of frequencies that has to be considered turns out to depend on the plasma resistivity, or, equivalently, the magnetic diffusion. If the magnetic diffusion coefficient is small, the required number of frequencies is prohibitively large; use of a smaller number of discrete frequencies leads to solutions with a series of narrow high-amplitude peaks inside the magnetopause [*De Keyser*, 2000]. An alternative approach consists of solving the wave propagation equations as a time-dependent initial value/boundary value problem. In an earlier paper we have reported on such a simulation code [*De Keyser and Čadež*, 2001]. That paper focused on the development of a single resonant sheet in an unperturbed low-beta plasma upon incidence of a monochromatic wave. It demonstrated that the resonant amplitude initially grows exponentially, while it saturates later on because of diffusive effects. The present paper uses the same code to compute the response of the magnetopause to intermittent and broadband waves. In doing so, we overcome the limitations of the Fourier mode decomposition approach: We find enhanced fluctuation levels throughout the magnetopause transition, while the fluctuation amplitude never becomes excessively high. The simulations presented here are quite realistic in spite of a number of model limitations. The simulation techniques allow for a quantitative estimate of the wave energy transmitted into the magnetosphere and of the energy that is resonantly absorbed at the magnetopause.

There is some literature on broadband driving of MHD systems that are characterized by discrete eigenmodes [e.g., *Poedts and Kerner*, 1992; *Wright and Rickard*, 1995]. These studies show how a broadband driver may excite such discrete eigenmodes. What we present here is different: We study how a continuous subspectrum of the system under study is excited by broadband waves. Moreover, we also consider intermittency of the driver.

## 2. Magnetohydrodynamic Description

A dissipationless plasma configuration in which a magnetic field aligned slab-like nonuniformity separates two regions with distinct plasma properties, can support MHD waves that propagate across the slab as well as Alfvén and slow waves that propagate parallel to the slab. Such modes propagate in individual magnetic plane surfaces parallel to the slab and are therefore called "local modes". Resonant MHD mode conversion occurs when an incident magnetoacoustic MHD wave that propagates toward and into the slab nonuniformity arrives at a location where its phase matches that of local MHD modes. Consequently, the local mode starts resonating with the incoming wave and the wave amplitude grows there, forming a resonant sheet. The resonant amplitude remains bounded by dissipation and by nonlinear effects. Dissipation causes the local mode to transfer its energy to the plasma by heating it in the resonant layer. The net effect is that a fraction of the incident wave energy is resonantly absorbed.

We consider the mechanism of resonant absorption of linear MHD waves in a weakly dissipative hydrogen plasma in the low-beta approximation. We adopt the same typical subsolar magnetopause configuration as in our earlier paper [*De Keyser and Čadež*, 2001]. The direction of nonuniformity is along $x$; the plasma slab is parallel to the $yz$ plane. Let $\rho$ denote the mass density, $\boldsymbol{v}$ the bulk velocity, $\boldsymbol{j}$ the current density, and $\boldsymbol{B}$ and $\boldsymbol{E}$ the magnetic and electric fields. The unperturbed state is a static equilibrium ($\boldsymbol{v}^{(0)} \equiv \boldsymbol{0}$) in which the magnetic field $B^{(0)} = 50$ nT is constant because of pressure balance, unidirectional along $z$, and therefore parallel to the slab. Gravitational effects are not taken into account. The density (Figure 1a) varies across the slab as

$$\rho^{(0)}(x) = \rho_{\mathrm{msph}}\mathcal{G}(x/D) + \rho_{\mathrm{msh}}\mathcal{G}(-x/D),$$

where $\mathcal{G}(x/D) = \frac{1}{2}\,\mathrm{erfc}\,(x/D)$ (erfc is the complementary error function), modeling a magnetopause with half width $D = 300$ km [*Berchem and Russell*, 1982], and where $\rho_{\mathrm{msph}}/m = 1$ cm$^{-3}$ and $\rho_{\mathrm{msh}}/m = 20$ cm$^{-3}$ ($m$ is the proton plus electron mass). The Alfvén speed $v_A = B^{(0)}/(\mu_0\rho^{(0)})^{1/2}$ changes from 244 to 1091 km s$^{-1}$ from magnetosheath to magnetosphere (Figure 1b).

The continuity and low-beta momentum equations are

$$\frac{\partial\rho}{\partial t} + \nabla\cdot(\rho\boldsymbol{v}) = 0, \tag{1}$$

$$\frac{\partial\rho\boldsymbol{v}}{\partial t} + \nabla\cdot\left[\rho\boldsymbol{v}\boldsymbol{v} + \frac{B^2}{2\mu_0}\boldsymbol{I} - \frac{1}{\mu_0}\boldsymbol{B}\boldsymbol{B}\right] = \boldsymbol{0}. \tag{2}$$

where $\boldsymbol{I}$ is the unit tensor. The generalized Ohm's law is

$$\boldsymbol{E} + \boldsymbol{v}\times\boldsymbol{B} = \eta\mu_0\boldsymbol{j}, \tag{3}$$

with $\mu_0\eta$ the electric resistivity; $\eta$ is the magnetic diffusivity. Maxwell's equations become

$$\nabla\times\boldsymbol{B} = \mu_0\boldsymbol{j}, \tag{4}$$

$$\frac{\partial\boldsymbol{B}}{\partial t} + \nabla\times\boldsymbol{E} = \boldsymbol{0}, \tag{5}$$

$$\nabla\cdot\boldsymbol{B} = 0. \tag{6}$$

The solution is assumed to consist of a one-dimensional equilibrium $\boldsymbol{q}^{(0)}(x)$ upon which small-amplitude waves $\boldsymbol{q}^{(1)}(x,y,z,t)$ are superimposed. We limit ourselves to harmonic variations in the $y$ and $z$ directions (parallel to the slab): $q^{(1)}(x,y,z,t) = \hat{\boldsymbol{q}}(x,t)\exp i(k_y y + k_z z)$, where $k_y$ and $k_z$ are given tangential wave numbers. The linearized equations form a homogeneous system of partial differential equations in $x$ and $t$:

$$\left(\frac{1}{v_A}\frac{\partial}{\partial t} + \boldsymbol{\mathcal{A}}_x\frac{\partial}{\partial x}\right)\boldsymbol{q}^{(1)} = (\eta\boldsymbol{\mathcal{C}}\nabla^2 - ik_y\boldsymbol{\mathcal{A}}_y - ik_z\boldsymbol{\mathcal{A}}_z)\boldsymbol{q}^{(1)} \tag{7}$$

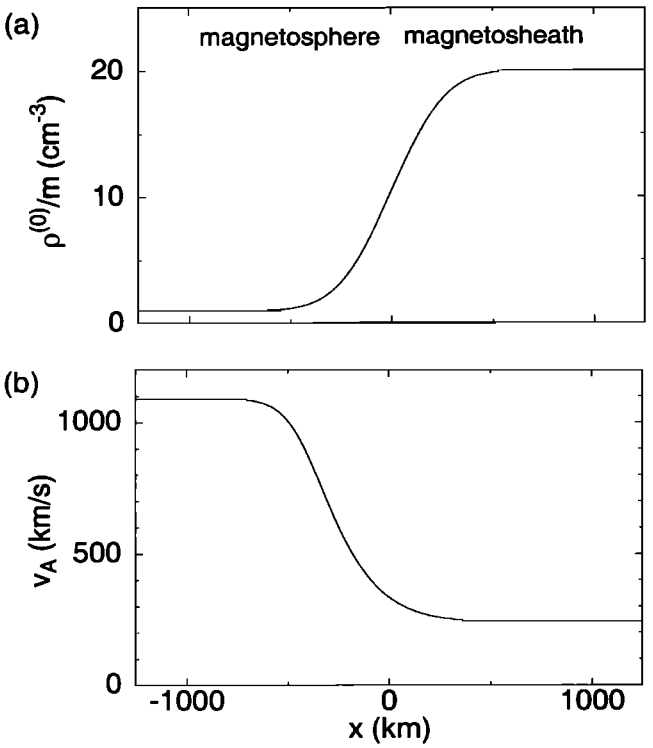


**Figure 1.** In a low-beta plasma with a constant and unidirectional magnetic field, the subsolar magnetopause equilibrium is fully determined by (a) the density profile, with a characteristic half width of 300 km, that is responsible for (b) the Alfvén speed variation across the layer. The magnetosphere in this and subsequent plots is always to the left, the magnetosheath to the right.

with $\boldsymbol{q}^{(1)} = [v_x^{(1)}, v_y^{(1)}, B_x^{(1)}, B_y^{(1)}, B_z^{(1)}]$, and where

$$\boldsymbol{\mathcal{A}}_x = \begin{bmatrix} \cdot & \cdot & \cdot & \cdot & b^{-2} \\ \cdot & \cdot & \cdot & \cdot & \cdot \\ \cdot & \cdot & \cdot & \cdot & \cdot \\ \cdot & \cdot & \cdot & \cdot & \cdot \\ b^2 & \cdot & \cdot & \cdot & \cdot \end{bmatrix}, \quad \boldsymbol{\mathcal{A}}_y = \begin{bmatrix} \cdot & \cdot & \cdot & \cdot & \cdot \\ \cdot & \cdot & \cdot & \cdot & b^{-2} \\ \cdot & \cdot & \cdot & \cdot & \cdot \\ \cdot & \cdot & \cdot & \cdot & \cdot \\ \cdot & b^2 & \cdot & \cdot & \cdot \end{bmatrix},$$

$$\boldsymbol{\mathcal{A}}_z = \begin{bmatrix} \cdot & \cdot & -b^{-2} & \cdot & \cdot \\ \cdot & \cdot & \cdot & -b^{-2} & \cdot \\ -b^2 & \cdot & \cdot & \cdot & \cdot \\ \cdot & -b^2 & \cdot & \cdot & \cdot \\ \cdot & \cdot & \cdot & \cdot & \cdot \end{bmatrix}, \quad \boldsymbol{\mathcal{C}} = \begin{bmatrix} \cdot & \cdot & \cdot & \cdot & \cdot \\ \cdot & \cdot & \cdot & \cdot & \cdot \\ \cdot & \cdot & 1 & \cdot & \cdot \\ \cdot & \cdot & \cdot & 1 & \cdot \\ \cdot & \cdot & \cdot & \cdot & 1 \end{bmatrix},$$

and $b^2 = B^{(0)}/v_A$. Neither the electric nor the magnetic force has a field-aligned component; as thermal forces are ignored in the low-beta case, it is found that $v_z^{(1)} \equiv 0$.

Let angle brackets denote averaging over the $y$ and $z$ dimensions. We define an energy density

$$\mathcal{E} = \rho^{(0)}\langle v^{(1)2}\rangle/2 + \langle B^{(1)2}\rangle/2\mu_0$$

and a corresponding energy flux

$$\phi_x = (B^{(0)}/\mu_0)\langle v_x^{(1)} B_z^{(1)}\rangle$$

that satisfy a conservation law

$$\frac{\partial \mathcal{E}}{\partial t} + \frac{\partial \phi_x}{\partial x} = 0.$$

Equations (7) contain the aforementioned local modes that do not propagate along the $x$ direction but remain bounded to $yz$ planes. No convective $x$ flux is associated with them: $\boldsymbol{\mathcal{A}}_x \partial \boldsymbol{q}^{(1)}/\partial x \equiv \boldsymbol{0}$. The dispersion relation of such local modes with frequency $\omega$ in a dissipationless medium then follows from (7)

$$\omega^2(x) - k_z^2 v_A^2(x) = 0,$$

representing a continuous spectrum of local Alfvén waves. Phase matching between an incoming wave with frequency $\omega$ and this continuum occurs at planes $x = x^*$ where the Alfvén resonance condition is satisfied,

$$v_A(x^*) = \pm\omega/k_z. \tag{8}$$

When thermal pressure is not negligible, resonances with slow waves can also occur [*Goossens and Ruderman*, 1995; *Čadež et al.*, 1997; *De Keyser et al.*, 1999].

Equations (7) form a linear hyperbolic problem. For a detailed account of the numerical solver we refer the interested reader to our previous paper [*De Keyser and Čadež*, 2001]. We use a finite volume mesh, a numerical flux with second-order reconstruction and with a minmod flux limiter, and Heun's method as time integrator. The simulations are second-order accurate in space and time. The mesh must be sufficiently fine so as to resolve the wavelengths involved; the integration time step is then automatically chosen to resolve the corresponding wave periods. We numerically integrate the wave propagation equations across the resonant layer rather than using the classical connection formulae across resonances [*Sakurai et al.*, 1991; *Goossens et al.*, 1995; *Goossens and Ruderman*, 1995]. We make sure that the spatial and temporal accuracy are high enough so as to obtain mesh-independent results.

## 3. Initial and Boundary Conditions

We solve equations (7) as an initial value/boundary value problem. The system is initially unperturbed. The boundary conditions are specified by time series that describe the incoming waves at the magnetospheric and magnetosheath edges of the domain. In what follows, no waves enter the simulation domain from the magnetospheric side; only waves incident from the magnetosheath are present. While any arbitrary perturbation can be specified as magnetosheath boundary condition, only those perturbation components for which the magnetosheath dispersion relation yields a real $k_x$ can propagate into the domain; the other components are evanescent.

In a low-beta plasma the incident waves can be Alfvén or fast waves. However, the condition for mode resonance in the inhomogeneity can only be satisfied for an incident fast wave. We consider three types of incident waves: (1) First we look at a superposition of two monochromatic fast waves that enter the solution domain at time $t_0 = 0$; this is a proto-

type of broadband waves. (2) We then consider a monochromatic fast wave pulse as an example of intermittency. (3) We finally use intermittent broadband magnetosheath waves observed by satellites in situ.

Incident waves with circular frequency $\omega = 2\pi f$ and wave vector $\boldsymbol{k} = [k_x, k_y, k_z]$ satisfy the magnetosheath dispersion relation

$$(\omega^2 - k_z^2 v_{A,\mathrm{msh}}^2)(\omega^2 - k^2 v_{A,\mathrm{msh}}^2) = 0,$$

which can readily be derived from equation (7). The first and the second factor correspond to the Alfvén and the fast magnetoacoustic mode, respectively. For given $\omega$, $k_y$, and $k_z$, a fast wave propagates if $k_x^2 = \omega^2/v_{A,\mathrm{msh}}^2 - k_y^2 - k_z^2 > 0$. A monochromatic fast wave (used in the construction of the dual-frequency and wave pulse boundary conditions) has the form

$$\begin{aligned}
\hat{v}_{x,y}(x_{\mathrm{msh}}, t) &= -\frac{k k_{x,y}}{k^2 - k_z^2} \frac{B_{\mathrm{ref}}}{B^{(0)}} v_{A,\mathrm{msh}} \sin(\omega t), \\
\hat{B}_{x,y}(x_{\mathrm{msh}}, t) &= -\frac{k_{x,y} k_z}{k^2 - k_z^2} B_{\mathrm{ref}} \sin(\omega t), \\
\hat{B}_z(x_{\mathrm{msh}}, t) &= -B_{\mathrm{ref}} \sin(\omega t),
\end{aligned}$$

where $B_{\mathrm{ref}}$ is a scaling constant.

## 4. Dual-Frequency Waves

In order to examine the role of the broad frequency spectrum of the incident perturbations, we consider a driver that consists of two propagating fast wave components at different frequencies. In that case

$$k_{x,\mathrm{msh}}^2 = \omega^2/v_{A,\mathrm{msh}}^2 - k_y^2 - k_z^2 > 0$$

for each frequency component, where $k_y$ and $k_z$ are the same for both components. This implies different $k_x$ and hence different incidence angles. The higher the frequency, the closer the component will be to normal incidence. A velocity dispersion therefore occurs in the $x$ direction (faster propagation along $x$ when $\alpha$ smaller). A component propagates through the magnetosphere if

$$k_{x,\mathrm{msph}}^2 = \omega^2/v_{A,\mathrm{msph}}^2 - k_y^2 - k_z^2 > 0.$$

Partial transmission across the magnetopause can occur if

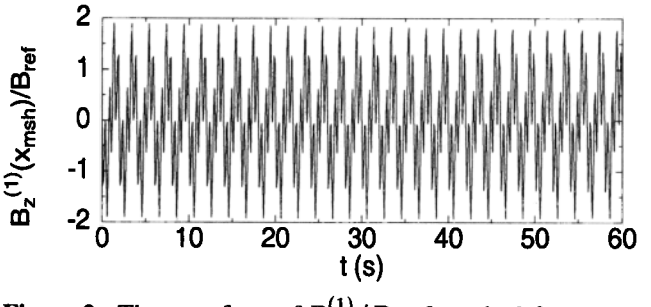


**Figure 2.** The waveform of $B_z^{(1)}/B_{\mathrm{ref}}$ for a dual-frequency incident wave with a component at frequency $f_1 = 0.5\,\mathrm{Hz}$, incidence angles $\phi = 135°$ and $\theta = 45°$, and a component at $f_2 = 2\,\mathrm{Hz}$.

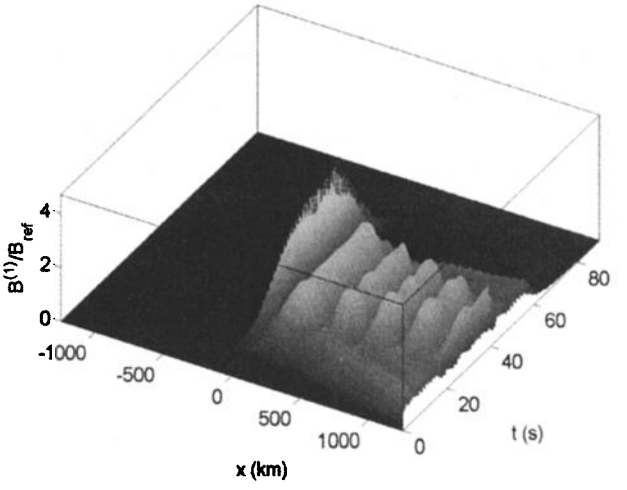


**Figure 3.** Magnetic field perturbation $B^{(1)}(x, 0, 0, t)/B_{\mathrm{ref}}$ for the incident wave of Figure 2. The 0.5 Hz component is partially reflected and partially resonantly absorbed, while the 2 Hz component is partially reflected and partially transmitted. The transmission is evident as the nonzero magnitude in the magnetospheric half of the domain ($x < 0$). There is a single resonant peak in the magnetopause (near $x = 0$). The growth and the saturation of the magnetic field perturbation amplitude in the resonant sheet are clearly visible.

$$\frac{v_{A,\mathrm{msh}}^2}{v_{A,\mathrm{msph}}^2} = \frac{\rho_{\mathrm{msph}}}{\rho_{\mathrm{msh}}} > 1 - \cos^2\phi \cos^2\theta = \sin^2\alpha,$$

where $\phi$ is the azimuth of the wave vector (angle between $[k_x, k_y, 0]$ and the magnetopause normal) and $\theta$ its elevation (angle between $\boldsymbol{k}$ and the $xy$ plane), and where $\alpha$ is the angle between $\boldsymbol{k}$ and the slab normal. This condition depends on the incidence angles alone. For the equilibrium considered here, transmission occurs when $\alpha \leq 13°$.

As an example, we choose the first component to have frequency $f_1 = 0.5\,\mathrm{Hz}$ and incidence angles $\phi = 135°$ and $\theta = 45°$ ($\alpha = 60°$), which fixes the values of $k_y$ and $k_z$. The second component has a relatively high frequency $f_2 = 2\,\mathrm{Hz}$, implying nearly normal incidence. Both components are taken to have equal amplitude. The waveform of the incident waves is given in Figure 2. Figure 3 shows the magnetic field perturbation magnitude $B^{(1)}(x, y = 0, z = 0, t)/B_{\mathrm{ref}}$ as a function of distance $x$ from the center of the magnetopause and time $t$. Because of the linearity of the problem, this is the superposition of the perturbations obtained for each of the wave components individually. While the $f_1$ component is partially reflected and absorbed at the resonance (since $\alpha = 60°$), the $f_2$ component is partially reflected and transmitted ($\alpha \sim 0°$). The initial exponential growth and the saturation of the resonant layer due to diffusive effects are clearly visible. The amplitude modulation of the incident perturbation in the magnetosheath ($x > 0$) is due to the superposition of the two incident and the two reflected components. The nonzero amplitude in the magnetosphere ($x < 0$) corresponds to the transmitted component. The resonant amplitude peak is found inside the magnetopause. The saturation amplitude and the saturation time

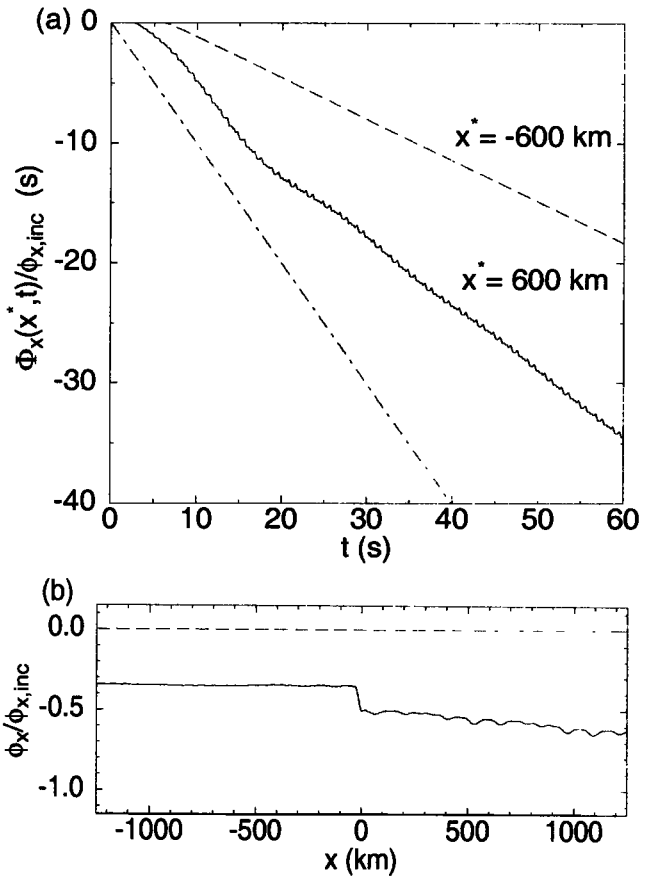


**Figure 4.** Same problem as in Figure 3: (a) Time-integrated energy flux $\Phi_x$ at various positions $x^*$, normalized to the average incident energy flux $\phi_{x,\mathrm{inc}}$. The dot-dashed line represents the time-integrated incident flux. (b) Spatial profile of the normalized time-averaged energy flux $\phi_x/\phi_{x,\mathrm{inc}}$ during saturation, showing transmission (nonzero flux in the magnetosphere), absorption (sharp flux change at the resonance), and partial transmission ($0 < \phi_x/\phi_{x,\mathrm{inc}} < 1$ in the magnetosheath).

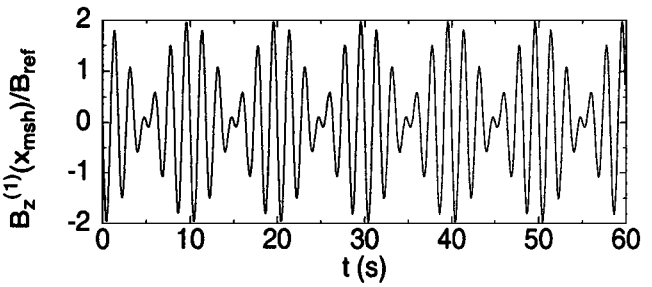


**Figure 5.** The waveform of $B_z^{(1)}/B_{\mathrm{ref}}$ for a dual-frequency incident wave with a component at frequency $f_1 = 0.5$ Hz, incidence angles $\phi = 135°$ and $\theta = 45°$, and a component at $f_2 = 0.6$ Hz; the waveform features an amplitude modulation at the wave-beating frequency $\Delta f = f_2 - f_1 = 0.1$ Hz.

both scale with $\eta^{-1/3}$, while the resonant sheet has a saturation thickness that scales with $\eta^{1/3}$ [*Kappraff and Tataronis*, 1977; *Poedts et al.*, 1990; *De Keyser and Čadež*, 2001]. The behavior of the system can easily be understood in terms of the energy transport. Initially, the incident wave transports energy toward the magnetopause. A fraction of it is transmitted across the layer, another fraction is reflected, while the remainder is resonantly absorbed. At first, the resonantly absorbed energy is mainly stored in the local waves, and their amplitude grows. As the amplitude variations in the narrow layer become more important with time, however, dissipative effects progressively become more pronounced, until the resonantly absorbed energy is completely balanced by the Ohmic dissipation. Figure 4a plots the time-integrated incident flux

$$\Phi_x(x^*,t) = \int_{\tau=0}^{t} \phi_x(x^*,\tau)/\phi_{x,\mathrm{inc}} d\tau$$

at $x^* = -600$ and 600 km, normalized to the incident flux $\phi_{x,\mathrm{inc}}$. $\Phi_x(x^*,t)$ represents the energy that has crossed the magnetic surface at $x^*$ since the beginning of the simulation (negative sign indicates transport from magnetosheath to magnetosphere). The dot-dashed line with slope $-1$ corresponds to the energy fed to the system by the incident wave. The solid line ($x^* = 600$ km) remains zero until $t = 3$ s, at which time the incident wave front reaches this position. Until $t = 18$ s the slope remains approximately $-1$ as only incident waves are present here. In the meantime, the leading wave front propagates further to the magnetopause and is partially reflected there. At $t = 18$ s the reflected wave front arrives back at $x^*$; since it carries energy in the opposite direction, the slope is reduced. At about the same time the resonance reaches saturation. The dashed line ($x^* = -600$ km) shows the constant transmitted flux. The final state of the system is depicted in Figure 4b. The normal energy flux $\phi_x$ in the saturated regime, time-averaged over a common multiple of both wave periods and normalized to the incident flux, is earthward (negative) everywhere. About 35% of the incident flux is transmitted, 40% is reflected, while 25% is resonantly absorbed (the jump at the

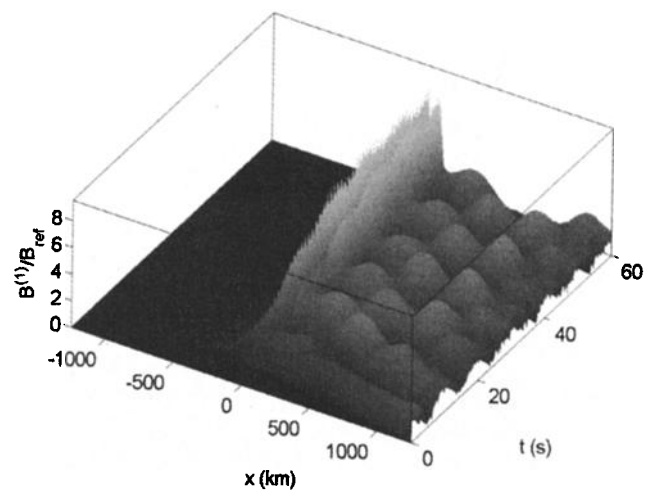


**Figure 6.** Magnetic field perturbation $B^{(1)}(x,0,0,t)/B_{\mathrm{ref}}$ generated by the incident wave of Figure 5. Each of the two components gives rise to a resonant sheet. The magnetic field perturbation amplitude in the resonant sheets is modulated because of wave beating.

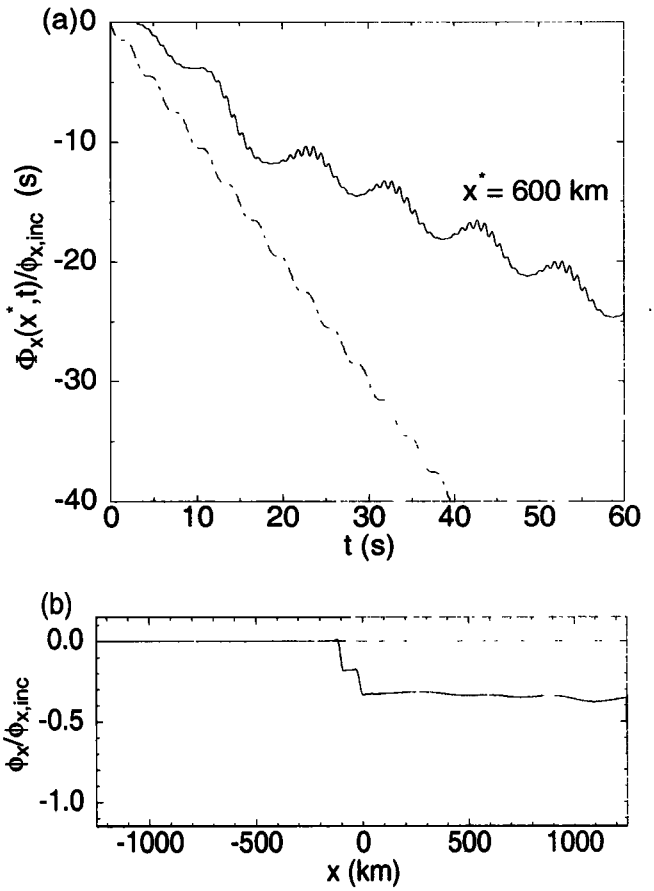


**Figure 7.** Same problem as in Figure 6: (a) Time-integrated energy flux $\Phi_x$ at $x^* = 600$ km, normalized to the average incident energy flux $\phi_{x,\mathrm{inc}}$. The dot-dashed line represents the time-integrated incident flux. (b) Spatial profile of the normalized time-averaged energy flux $\phi_x/\phi_{x,\mathrm{inc}}$ during saturation, showing the absence of transmission (zero flux in the magnetosphere) and two sites of absorption (sharp flux change at each resonance).

resonant layer). Note that there is some dissipative damping of the incident wave as it traverses the magnetosheath (which depends on the diffusion constant used in the simulation).

In another example we keep the first component the same ($f_1 = 0.5$ Hz) but we choose a nearby frequency for the second component ($f_2 = 0.6$ Hz). The incident wave features an amplitude modulation at the beating frequency $\Delta f = f_2 - f_1 = 0.1$ Hz (Figure 5). Figure 6 shows the time evolution of the system. There is no transmission. Two resonant peaks are formed inside the magnetopause, one for each frequency component. The perturbation magnitudes at both resonances are modulated at the beating frequency. The time-integrated flux (Figure 7a) shows how a quasi-steady situation arises after saturation is reached. At times the net magnetosheath energy flux is sunward (positive) rather than earthward (negative), an effect due to wave beating. The energy flux profile has two steep steps, corresponding to the absorbed wave power at each resonance (Figure 7b); more than 30% of the incident flux is absorbed.

Dual-frequency waves are the first step toward broadband waves. The results obtained in this section suggest that incident perturbations with a broad frequency spectrum imply that resonant fluctuations are excited at different places throughout the magnetopause, depending on the frequencies present in the incident wave spectrum.

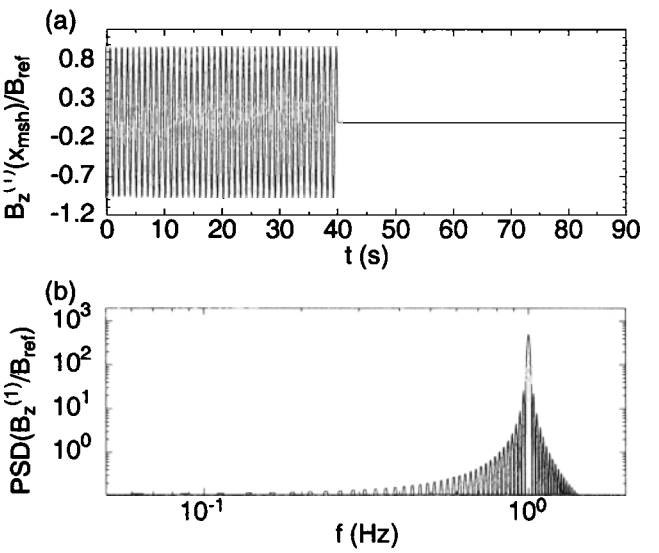


**Figure 8.** Characteristics of an incident monochromatic wave pulse with frequency $f = 1$ Hz and incidence angles $\phi = 135°$ and $\theta = 45°$ that lasts 40 s. (a) The waveform of the $z$ component of the magnetic perturbation and (b) its power spectral density, showing a main peak at frequency $f$.

## 5. Monochromatic Wave Pulse

As a prototype of intermittency, we consider a monochromatic wave pulse of limited duration. The abrupt beginning and end of the pulse add a broad high-frequency spectrum to the single frequency of the wave inside the pulse. The longer the pulse duration, the more pronounced the spectral peak at this frequency will be.

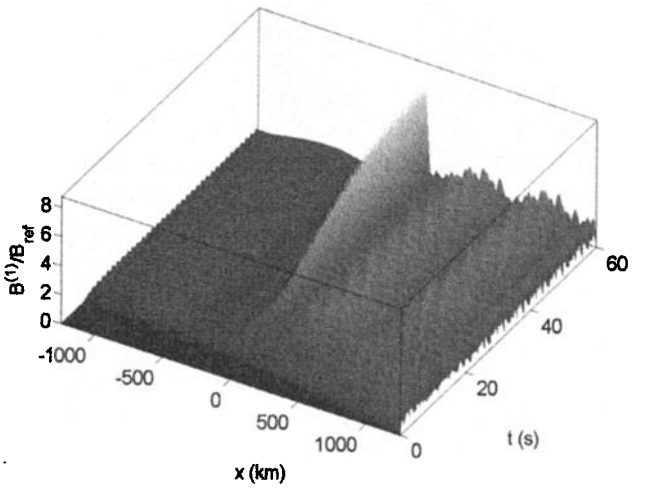


**Figure 9.** Magnetic field perturbation $B^{(1)}(x,0,0,t)/B_{\mathrm{ref}}$ generated by the incident wave of Figure 8. The pulse lasts long enough to drive the resonance into the saturation regime. Once the pulse stops, the perturbation amplitude starts to decay with time.

Figure 8a shows a monochromatic wave pulse ($f = 1$ Hz, $\phi = 135°$ and $\theta = 45°$, $\alpha = 60°$) lasting 40 wave periods. The incident wave has a peak power spectral density at frequency $f$ (Figure 8b). The magnetic field perturbation is shown in Figure 9. Upon arrival of the pulse at the transition, the resonant mode is excited. The pulse lasts long enough for the resonance to reach saturation. Once the incident pulse stops, the amplitude of the resonant mode starts to decay exponentially. Because the peak in the incident spectrum is so sharp, only a single resonant peak is formed. Saturation occurs after about $t = 30$ s, while the exponential decay begins at $t = 45$ s. This decay is due to diffusive damping of the excited local modes. The evolution of the system can again be understood in terms of energy transport. The dot-dashed line in Figure 10a represents the energy input into the system by the driver, which stops at $t = 40$ s. The solid line ($x^* = 600$ km) shows the initial propagation delay. It reaches a slope of $-1$ while only the incident wave is present. From $t = 18$ s on, the reflected wave carries energy back to the magnetosheath. The slope is still negative as the incident flux remains larger than the reflected flux: There is no transmission, but energy is stored in the local mode at the resonance. Near $t = 30$ s the resonance is almost saturated as the resonantly absorbed energy matches the dissipative loss in the layer. At $t = 45$ s the driver stops: The slope of the $\Phi_x(x^*, t)$ profile becomes positive as only reflected waves are present. After $t = 55$ s, there is no more wave activity at $x^* = 600$ km and the system returns to its original unperturbed state. However, the $\Phi_x(x^*, t)$ curve does not return to the zero level: In the course of time, the system has irreversibly converted incident wave energy into Ohmic heat. Figure 10b shows the net energy flux averaged over the whole duration of the simulation. There is a relatively minor amount of resonantly absorbed energy (10%): The resonance was barely driven to saturation, while dissipation is strongest at saturation.

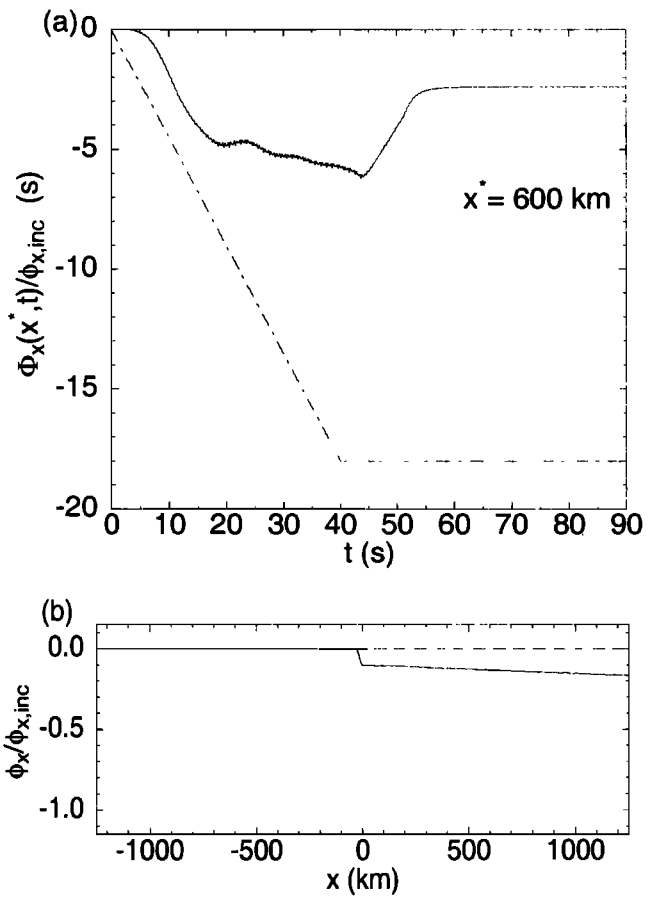


**Figure 10.** Same problem as in Figure 9: (a) Time-integrated energy flux $\Phi_x$ at $x^* = 600$ km, normalized to the average incident energy flux $\phi_{x,\mathrm{inc}}$ in the monochromatic pulse. The dot-dashed line represents the time-integrated incident flux; no more energy is added to the system after the incident pulse stops. (b) Spatial profile of the normalized energy flux $\phi_x/\phi_{x,\mathrm{inc}}$ averaged over the whole simulation, showing that transmission is essentially absent (zero flux in the magnetosphere), while some absorption has occurred at the resonance. The remainder of the incident flux is reflected.

In summary, intermittency of magnetosheath waves leads to the turning on and off of mode conversion. Space plasmas are characterized by small $\eta$, so that the saturation timescale is rather long as it scales with $\eta^{-1/3}$. The incident wave component at one particular frequency should therefore last rather long for the resonant mode to reach saturation. When the driver starts, there is a growth period; when it stops, the wave amplitude decays. Therefore the local modes present in the magnetopause at any given moment reflect the recent history of the incident waves.

## 6. Observed Magnetosheath Waves

We now consider wave observations in the subsolar magnetosheath by the Active Magnetospheric Particle Tracer Explorers (AMPTE) Ion Release Module (IRM) on September 16, 1984, from 0205 to 0220 UT, shortly after the satellite left the magnetosphere through a rather low magnetic shear magnetopause (less than 90° magnetic field rotation). The wave activity during this selected time interval is typical. The magnetic field and plasma variations were not too large, so that a linear approximation is not unreasonable. We specified the observed GSE $B_x$, $B_y$, $B_z$, $v_x$, and $v_y$ variations (at a 0.2 Hz sampling rate) around their mean value as the perturbations in the boundary conditions. Although the magnetic field was not unidirectional along $z$, we did not realign the $z$ axis with the actual magnetic field direction. The low-beta approximation is also not completely justified. The satellite observations do not give much information on the propagation directions of the waves. What is measured is the sum of incident and reflected waves, rather than the incident waves alone. We therefore can not fully reconstruct the wave environment at the magnetopause. Nevertheless, the data do give a realistic impression of the intermittency of magnetosheath waves.

As already discussed, the simulation requires given fixed values for $k_y$ and $k_z$, thus imposing a systematic variation of the incidence angles with frequency. We have chosen $k_y = k_z = 5 \times 10^{-7}\,\mathrm{m}^{-1}$, which allows propagation for frequencies $\gtrsim 0.028$ Hz (about the sampling frequency) in the magnetosheath, and $\gtrsim 0.12$ Hz in the magnetosphere. Waves with this $k_y$ and $k_z$ and with frequencies below 0.028 Hz

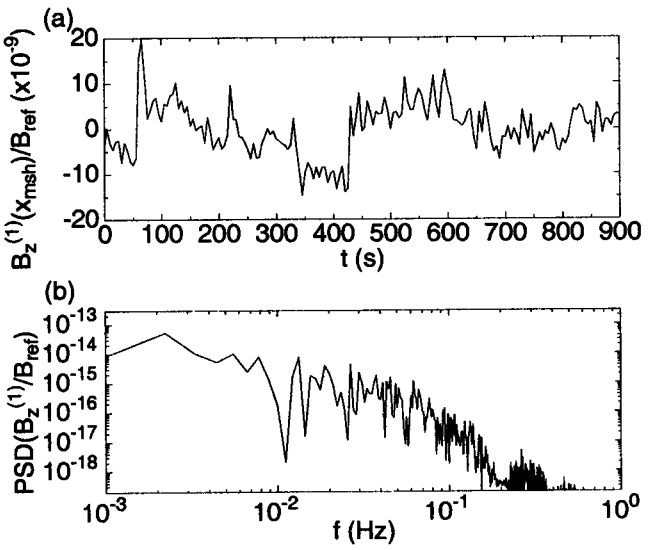


**Figure 11.** Characteristics of incident waves observed by the Active Magnetospheric Particle Tracer Explorers (AMPTE) Ion Release Module (IRM) in the magnetosheath on September 16, 1984, from 0205 to 0220 UT. The sampling frequency was 0.2 Hz. (a) The waveform of the $z$ component of the magnetic field perturbation, and (b) its power spectral density, illustrating the broad frequency content of the signal. The power spectral density drops quickly beyond the sampling frequency; the higher frequencies arise as a consequence of interpolating the signal.

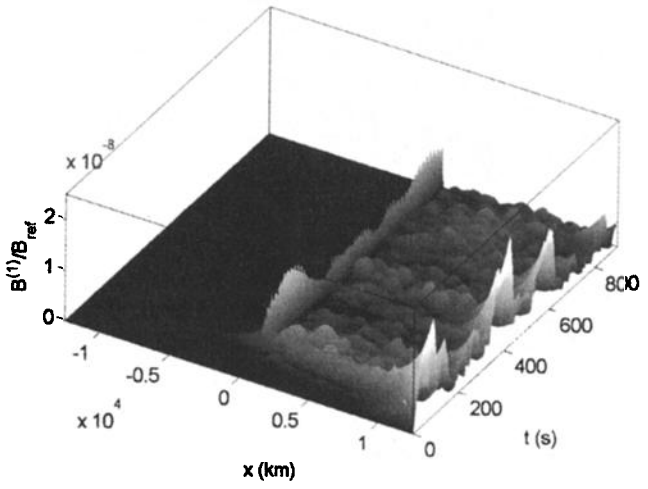


**Figure 12.** Magnetic perturbation $B^{(1)}(x,0,0,t)/B_{\rm ref}$ generated by the incident wave of Figure 11. The tangential wave vector components were chosen as $k_y = k_z = 5 \times 10^{-7}\,\mathrm{m}^{-1}$. The time axis covers a period of 900 s. The spatial domain extends about $2\,R_E$ on either side of the magnetopause. The fluctuation level in the magnetopause changes with time and loosely follows the wave activity in the magnetosheath.

are evanescent in the magnetosheath, those with frequencies in the 0.028–0.12 Hz range experience partial reflection and resonant amplification, and those above 0.12 Hz are partially transmitted and reflected ($\alpha \sim 0$) but cannot be resonantly amplified. Figure 11 plots the observed $B_z$ waveform and its power spectral density. The incident waves display a few strong sudden changes, as well as longer lasting low-amplitude fluctuations. Much of the spectral power is present in the 0.01-0.1 Hz range. The frequency spectrum rapidly drops off beyond the 0.2 Hz sampling frequency; the higher-frequency part of the spectrum is introduced by interpolation as the time integrator typically samples the boundary condition at a frequency above 1 kHz. Figure 12 shows the magnetic field perturbation magnitude as a function of space and time. As the relevant frequencies are an order of magnitude smaller than in the previous examples, the simulation domain has been extended to the region from -12,500 to 12,500 km. Computational complexity forced us to work with a relatively large diffusion $\eta = 10^8\,\mathrm{m}^2/\mathrm{s}$. The incident waves with frequencies below 0.028 Hz are evanescent, while those with frequencies above $f_{\rm high} = v_A^2/\eta \sim 500$ Hz are damped because of diffusion. As waves with frequencies above the sampling frequency 0.2 Hz are largely absent in the input signal, and as the choice of the tangential wave vector permits propagation in the magnetosphere only above 0.12 Hz, there is almost no transmission. Figure 13 zooms in on the perturbations near the magnetopause between $x$ =-1250 and 1250 km. Number and location of the resonant peaks continuously vary with time. Resonances rarely reach the constant-amplitude saturated regime. Figure 14a shows the maximum magnetic field magnitude as a function of distance of the magnetopause. The exponentially reduced amplitude at the magnetosheath edge is due to the wave components in the observational data that do not correspond to propagating magnetosheath waves in the simulation. This may seem strange, because these waves must necessarily be propagating in the magnosheath if they are observed there. However, their actual propagation direction is unknown and probably does not match our choice of $k_y$ and $k_z$. A clear feature is the enhanced fluctuation level at the magnetopause. Figure 14b plots the time-averaged en-

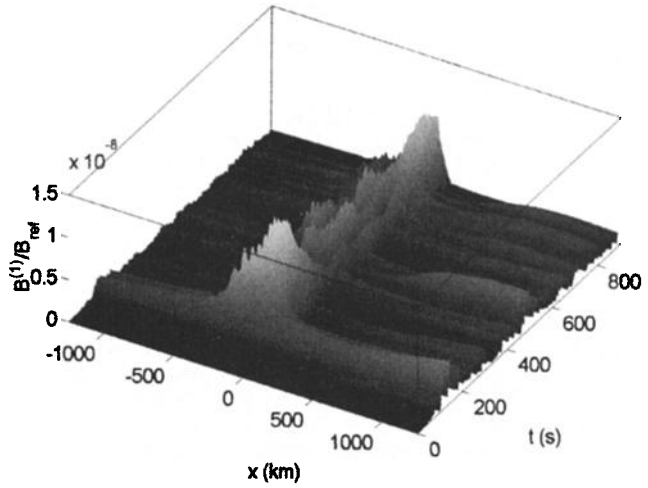


**Figure 13.** The same as Figure 12, but with $x$ ranging from -1250 to 1250 km. Resonant modes are excited to a different degree and at different locations in the magnetopause throughout the simulation, but they never are driven long enough so as to allow them to reach the saturation regime.

ergy flux, that is, the time-integrated energy flux over the whole simulation relative to the time-integrated flux input by the incident waves. We obtain some dissipative damping of waves in the magnetosheath. Resonant absorption occurs at the magnetopause, while there is also a small amount of transmission. In order to obtain a better view of what happens at the magnetopause, Figure 14c shows the maximum perturbation amplitude (over the 900 s simulation) in the region -1250 to 1250 km. Instead of sharp individual peaks, there is a broad amplitude enhancement that coincides with the region of Alfvén speed variation (see Figure 1b). This region is slightly shifted earthward with respect to the region of the strongest density gradient because of the nonlinear relation between $v_A$ and $\rho$. The broad enhancement is the net result of the time-changing instantaneous resonant patterns visible in Figure 13. This time dependency is illustrated by the variations of the maximum magnetic field perturbation magnitude in the magnetopause layer in Figure 14d. After an initial short propagation delay, resonances grow and decay continuously. Figure 14e shows that the time-averaged resonantly absorbed flux is delivered not just to a number of resonant layers, but to all of the plasma inside the magnetopause: The flux profile shows a broad, smooth transition. This result should be contrasted to the staircase profile obtained by *De Keyser* [2000, Figure 11a] for the case of magnetosheath waves with a discrete frequency spectrum.

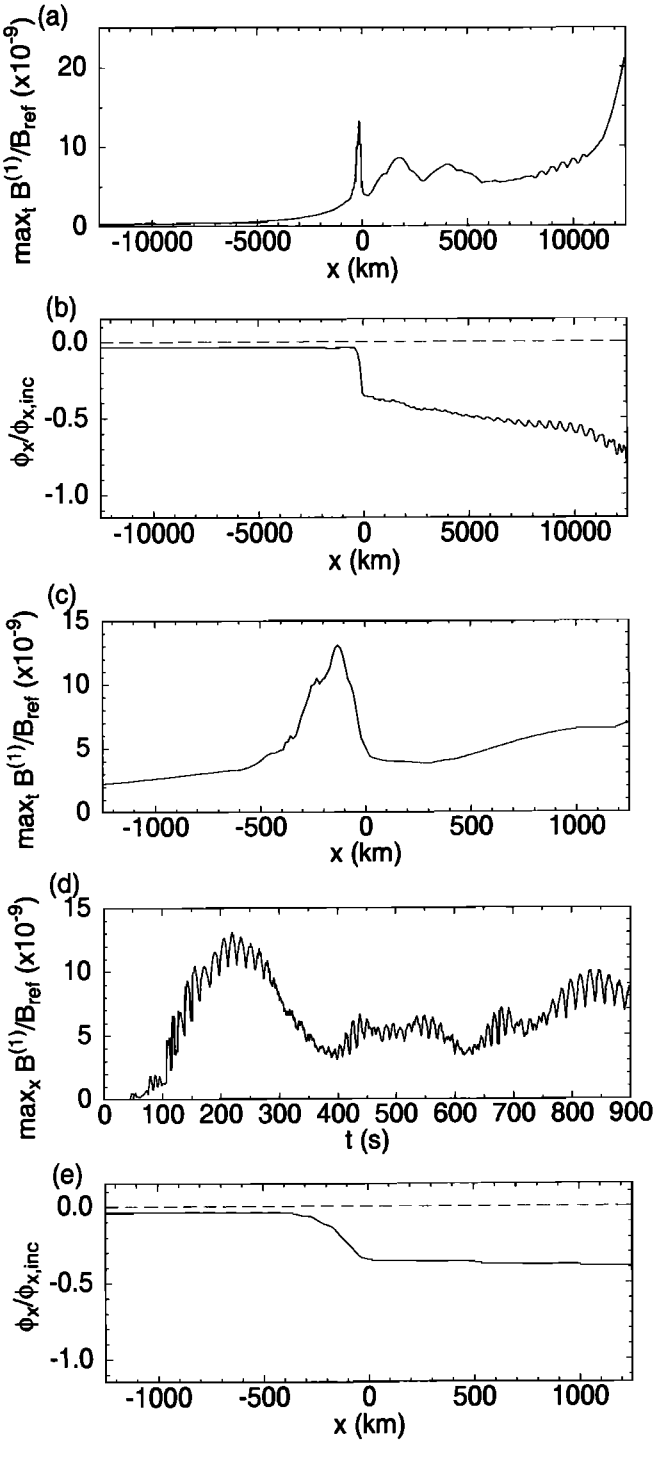


In conclusion, the fluctuation magnitudes are enhanced to a variable degree throughout the magnetopause, but they never exceed the incident fluctuation level by more than an order of magnitude. At the same time, enhanced perturbation magnitudes are found everywhere in the magnetopause layer. These findings precisely correspond to the observations [*Ness et al.*, 1966; *Perraut et al.*, 1979; *Rezeau et al.*, 1986].

## 7. Conclusions

We have presented simulations of the transient response of the magnetopause to intermittent broadband waves. First, we have analyzed the response for prototype incident waves: dual-frequency waves and monochromatic wave pulses. We then have used actual observations to mimic the intermittency and broadband nature of magnetosheath waves [*Anderson et al.*, 1982], in order to obtain a realistic and qualitative impression of the development of low-frequency fluctuations at the magnetopause. The results agree very well with observations of the fluctuation amplitude in the magnetosheath, the magnetopause, and the magnetosphere [*Ness et*

**Figure 14.** Same problem as in Figure 12: (a) Maximum magnitude of the magnetic perturbation during the whole simulation as a function of distance from the transition, $\max_t B^{(1)}(x,0,0)/B_{\rm ref}$, showing enhanced magnetic field fluctuations in the magnetopause. The decay in perturbation amplitude near the magnetosheath edge of the simulation domain is due to the presence of nonpropagating components in the incident waves, as well as due to diffusive damping of high-frequency components. (b) The overall normalized energy flux profile $\phi_x/\phi_{x,\rm inc}$ averaged over the whole simulation, showing partial transmission, partial resonant absorption, and partial reflection. (c) Magnetic perturbation amplitude, but now between $x = -1250$ and 1250 km. Enhanced amplitudes are found throughout the magnetopause. (d) Maximum magnitude of the magnetic field perturbation in the magnetopause as a function of time, $\max_{x,y,z} B^{(1)}(t)/B_{\rm ref}$. (e) The overall normalized energy flux profile $\phi_x/\phi_{x,\rm inc}$ averaged over the whole simulation between $x = -1250$ and 1250 km, showing resonant absorption throughout the magnetopause.

*al.*, 1966, Figures 2 and 3; *Perraut et al.*, 1979, Figures 2, 3, and 7; *Rezeau et al.*, 1986, Figure 1; *Song et al.*, 1993, Figures 3, 5, 8, and 11]. The contribution of this paper lies in its focus on resonant mode conversion as the underlying mechanism that is responsible for the enhancement of the field fluctuations at the magnetopause. The simulations illustrate that the broadband nature and the intermittency of the incident waves are essential for understanding why no sharp individual resonant sheets with extremely high perturbation amplitude are formed inside the magnetopause.

The approach in this paper is one-dimensional. We model wave propagation along $x$, the direction of the plasma inhomogeneity gradients, while we assume harmonic perturbations in the $y$ and $z$ directions with fixed $k_y$ and $k_z$. The ensuing frequency dependence of the incidence angles is artificial. While it is highly probable that waves in the magnetosheath are propagating in various directions, it is not necessarily so that the higher frequencies are systematically closer to normal incidence. The limitation of constant $k_y$ and $k_z$ could be overcome by spatial Fourier decomposition of the incident waves in the tangential directions; repeating our simulations for different values of $\omega$, $k_y$, and $k_z$ and superposing the results will give the desired answer, but this approach is difficult for continuous frequency and/or wave number spectra. The only alternative is to perform three-dimensional simulations, which are very compute-intensive.

The broadband intermittent linear MHD solution that we found here can readily be interpreted as a physically relevant wave propagation pattern. This stands in contrast to the very thin and very high amplitude resonant layers that are obtained for small $\eta$ for monochromatic drivers. While these individual resonant layers are properly defined solutions of the MHD equations, their physical relevance is not obvious a priori since their narrow width might be inferior to kinetic length scales (the ion gyroradius in particular), thus violating the basic MHD premises, and their amplitude might invalidate the small-amplitude assumption at the basis of the linearization approach.

The linear low-beta MHD analysis only considers frequencies well below the proton gyrofrequency. An extension of the present work to the case where thermal pressure cannot be ignored is straightforward. The inclusion of kinetic effects becomes inevitable above the proton gyrofrequency [*Lacombe et al.*, 1995; *Johnson and Cheng*, 1997]. In general, one should also resort to a nonlinear description of resonant absorption [*Ruderman et al.*, 1997]. The present model does not include any ionospheric coupling. The one-dimensional approximation becomes invalid for distances larger than a few Earth radii, when the magnetosheath flow away from the subsolar point and the curvature of the magnetopause cannot be ignored.

The enhanced fluctuation level as computed here is important for mass and energy transport across the magnetopause. Only a minor fraction of the incident wave energy is transmitted across the magnetopause. Some energy is resonantly absorbed and distributed throughout the magnetopause layer, while some is reflected. In MHD there can be no mass transport across the tangential discontinuity magnetopause, but kinetic effects such as wave-particle interactions are strongly enhanced for higher fluctuation levels, thus promoting diffusive mass transport across the magnetopause [*LaBelle and Treumann*, 1988; *Treumann et al.*, 1995]. Also, this diffusion might be what is required to initiate transient magnetic reconnection [e.g., *Ku and Sibeck*, 2000]).

While the present paper is focused on the magnetopause, the results are relevant for other fields of plasma physics as well. For instance, broadband incident waves in the solar corona could explain volume heating in coronal flux tubes as the resonant energy would be deposited throughout coronal inhomogeneities [*Poedts et al.*, 1989].

**Acknowledgments.** This work was supported by PRODEX in the framework of ESA's Cluster II mission and the Solar Drivers of Space Weather project. The authors gratefully acknowledge the support of the Belgian Federal Office for Scientific, Technical and Cultural Affairs.

Michel Blanc thanks Peter Gary and Marcel Goossens for their assistance in evaluating this paper.

## References

Anderson, B. J., and S. A. Fuselier, Magnetic pulsations from 0.1 to 4.0 Hz and associated plasma properties in the Earth's subsolar magnetosheath and plasma depletion layer, *J. Geophys. Res., 98*, 1461–1479, 1993.

Anderson, R. R., C. C. Harvey, M. M. Hoppe, B. T. Tsurutani, T. E. Eastman, and J. Etcheto, Plasma waves near the magnetopause, *J. Geophys. Res., 87*, 2087–2107, 1982.

Belmont, G., F. Reberac, and L. Rezeau, Resonant amplification of magnetosheath MHD fluctuations at the magnetopause, *Geophys. Res. Lett., 22*, 295–298, 1995.

Berchem, J., and C. T. Russell, The thickness of the magnetopause current layer: ISEE 1 and 2 observations, *J. Geophys. Res., 87*, 2108–2114, 1982.

Čadež, V. M., Á. Csík, R. Erdélyi, and M. Goossens, Absorption of magnetosonic waves in presence of resonant slow waves in the solar atmosphere, *Astron. Astrophys., 326*, 1241–1251, 1997.

Cahill, L. J., and P. G. Amazeen, The boundary of the geomagnetic field, *J. Geophys. Res., 68*, 1835–1843, 1963.

De Keyser, J., Linear magnetohydrodynamic response of the magnetopause to magnetosheath fluctuations, *J. Geophys. Res., 105*, 23,167–23,177, 2000.

De Keyser, J., and V. Čadež, Transient development of magnetohydrodynamic wave mode conversion layers, *J. Geophys. Res., 106*, 15,609–15,619, 2001.

De Keyser, J., M. Roth, F. Reberac, L. Rezeau, and G. Belmont, Resonant amplification of MHD waves in realistic subsolar magnetopause configurations, *J. Geophys. Res., 104*, 2399–2409, 1999.

Engebretson, M. J., N. Lin, W. Baumjohann, H. Lühr, B. J. Anderson, L.J. Zanetti, T.A. Potemra, R.L. McPherron, and M.G. Kivelson, A comparison of ULF fluctuations in the solar wind, magnetosheath, and dayside magnetosphere, 1, Magnetosheath morphology, *J. Geophys. Res., 96*, 3441–3454, 1991.

Goossens, M., and M. S. Ruderman, Conservation laws and connection formulae for resonant MHD waves, *Phys. Scr., T 60*, 171–184, 1995.

Goossens, M., M. S. Ruderman, and J. V. Hollweg, Dissipative MHD solutions for resonant Alfvén waves in 1-dimensional magnetic tubes, *Sol. Phys., 157*, 75–102, 1995.

Holzer, R. E., M. G. McLeod, and E. J. Smith, Preliminary results from the OGO 1 search coil magnetometer: Boundary positions and magnetic noise spectra, *J. Geophys. Res., 71*, 1481–1486, 1966.

Johnson, J. R., and C. Z. Cheng, Kinetic Alfvén waves and plasma

transport at the magnetopause, *Geophys. Res. Lett., 24*, 1423–1426, 1997.

Kappraff, J. M., and J. A. Tataronis, Resistive effects on Alfvén wave heating, *J. Plasma Phys., 18*, 209–226, 1977.

Ku, H. C., and D. G. Sibeck, Flux transfer events produced by the onset of merging at multiple X lines, *J. Geophys. Res., 105*, 2657–2675, 2000.

LaBelle, J., and R. A. Treumann, Plasma waves at the dayside magnetopause, *Space Sci. Rev., 47*, 175–202, 1988.

Lacombe, C., G. Belmont, D. Hubert, C. C. Harvey, A. Mangeney, C. T. Russell, J. T. Gosling, and S. A. Fuselier, Density and magnetic field fluctuations observed by ISEE 1-2 in the quiet magnetosheath, *Ann. Geophys., 13*, 343–357, 1995.

McKenzie, J. F., Hydromagnetic wave interaction with the magnetopause and the bow shock, *Planet. Space Sci., 18*, 1–23, 1970.

Ness, N. F., C. S. Scearce, and J. B. Seek, Initial results of the IMP 1 magnetic field experiment, *J. Geophys. Res., 69*, 3531–3569, 1964.

Ness, N. F., C. S. Scearce, and S. Cantarano, Preliminary results from the Pioneer 6 magnetic field experiment, *J. Geophys. Res., 71*, 3305–3313, 1966.

Perraut, S., R. Gendrin, P. Robert, and A. Roux, Magnetic pulsations observed onboard GEOS 2 in the ULF range during multiple magnetopause crossings, in Proceedings of the Magnetospheric Boundary Layers Conference, Alpbach, June 1979, *Eur. Space Agency Spec. Publ., ESA SP-148*, 113-122, 1979.

Poedts, S., and W. Kerner, Time scales and efficiency of resonant absorption in periodically driven resistive plasmas, *J. Plasma Phys., 47*, 139–162, 1992.

Poedts, S., M. Goossens, and W. Kerner, Numerical simulation of coronal heating by resonant absorption of Alfvén waves, *Sol. Phys., 123*, 83–115, 1989.

Poedts, S., M. Goossens, and W. Kerner, Temporal evolution of resonant absorption in solar coronal loops, *Comput. Phys. Commun., 59*, 95–103, 1990.

Rezeau, L., S. Perraut, and A. Roux, Electromagnetic fluctuations in the vicinity of the magnetopause, *Geophys. Res. Lett., 13*, 1093–1096, 1986.

Rezeau, L., A. Morane, S. Perraut, A. Roux, and R. Schmidt, Characterization of Alfvénic fluctuations in the magnetopause boundary layer, *J. Geophys. Res., 94*, 101–110, 1989.

Rezeau, L., A. Roux, and C. T. Russell, Characterization of small-scale structures at the magnetopause from ISEE measurements, *J. Geophys. Res., 98*, 179–186, 1993.

Ruderman, M. S., J. V. Hollweg, and M. Goossens, Nonlinear theory of resonant slow waves in dissipative layers, *Phys. Plasmas, 4*, 75–90, 1997.

Sakurai, T., M. Goossens, and J. V. Hollweg, Resonant behaviour of MHD waves on magnetic flux tubes, I, Connection formulae at the resonant surface, *Sol. Phys., 133*, 227–245, 1991.

Schwarz, S. J., D. Burgess, and J. J. Moses, Low-frequency waves in the Earth's magnetosheath: Present status, *Ann. Geophys., 14*, 1134–1150, 1996.

Song, P., C. T. Russell, and C. Y. Huang, Wave properties near the subsolar magnetopause: Pc 1 waves in the sheath transition layer, *J. Geophys. Res., 98*, 5907–5923, 1993.

Song, P., C. T. Russell, and S. P. Gary, Identification of low-frequency fluctuations in the terrestrial magnetosheath, *J. Geophys. Res., 99*, 6011–6025, 1994.

Southwood, D. J., Some features of field line resonances in the magnetosphere, *Planet. Space Sci., 22*, 483–491, 1974.

Treumann, R. A., J. LaBelle, and T. M. Bauer, Diffusion processes: An observational perspective, in *Physics of the Magnetopause, Geophys. Monogr. Ser.*, vol. 90, edited by P. Song et al., pp. 331–341, AGU, Washington, D. C., 1995.

Verzariu, P., Reflection and rarefaction of hydromagnetic waves at the magnetopause, *Planet. Space Sci., 21*, 2213–2225, 1973.

Wright, A. N., and G. J. Rickard, A numerical study of resonant absorption in a magnetohydrodynamic cavity driven by a broadband spectrum, *Astrophys. J., 444*, 458–470, 1995.

V. Čadež and J. De Keyser, Belgian Institute for Space Aeronomy, Ringlaan 3, B-1180 Brussels, Belgium. (Vladimir.Cadez@bira-iasb.oma.be; Johan.DeKeyser@bira-iasb.oma.be)

(Received March 14, 2001; revised May 9, 2001; accepted May 14, 2001.)